TASK QUARTERLY 15 No 3–4, 339–352

UNSTRUCTURED FINITE-VOLUME MESHES FOR TWO-DIMENSIONAL FLOW IN VARIABLY SATURATED POROUS MEDIA

KAZIMIERZ BURZYŃSKI[1] AND ADAM SZYMKIEWICZ[2]

[1]*Department of Hydraulic Engineering,*
Faculty of Civil and Environmental Engineering,
Gdansk University of Technology,
Narutowicza 11/12, 80-233 Gdansk, Poland
kazimierz.burzynski@wilis.pg.gda.pl

[2]*Department of Geotechnics, Geology and Marine Engineering,*
Faculty of Civil and Environmental Engineering,
Gdansk University of Technology,
Narutowicza 11/12, 80-233 Gdansk, Poland
adams@pg.gda.pl

(Received 25 May 2011; revised manuscript received 16 August 2011)

Abstract: This paper presents a numerical algorithm for solving the equation describing variably saturated flow in porous media. The algorithm is based on a control volume finite element approach and can be applied to two-dimensional unstructured meshes consisting of triangular elements. Two methods of defining the dual control volume grid are discussed. We also demonstrate that the method of calculating the average permeability at the control volume face significantly influences numerical results.

Keywords: finite volume method, Richards equation, unsaturated flow, unstructured mesh

1. Introduction

The motion of water in the uppermost layer of the Earth's crust is of interest to civil and environmental engineers, hydrologists, hydrogeologists and agronomists. This process is characterized by a strongly varying degree of water saturation in porous soils or rocks. The governing equation for flow in variably

saturated porous media is based on the mass conservation principle, which for a case without sources and sinks, can be written as follows:

$$\frac{\partial}{\partial t}(\rho\phi S)+\nabla\cdot(\rho\boldsymbol{v})=0 \tag{1}$$

where ρ is the water density, ϕ is the medium porosity, S is the water saturation, and $\boldsymbol{v}$ is the volumetric water flux (seepage velocity) defined according to the Darcy's law as:

$$\boldsymbol{v}=-\frac{\boldsymbol{k}}{\mu}(\nabla p-\rho\boldsymbol{g}) \tag{2}$$

where $\boldsymbol{k}$ is the permeability tensor, μ is the water viscosity, p is the water pressure, and $\boldsymbol{g}$ is the gravitational acceleration vector. The values of water pressure are typically given with respect to atmospheric pressure, *i.e.* $p=0$ at the groundwater table, $p<0$ in the unsaturated zone, and $p>0$ in the saturated zone. In this paper, we consider isotropic media, for which the permeability can be written as:

$$\boldsymbol{k}=k_s\,k_r(S)\,\boldsymbol{I} \tag{3}$$

where k_s is the intrinsic permeability depending on the pore space geometry, $k_r(S)$ is the relative permeability depending on the water saturation, and $\boldsymbol{I}$ is the unit tensor. In a fully water-saturated medium, relative permeability is equal to one, while under unsaturated conditions it decreases nonlinearly with a decrease in saturation. Moreover, in the unsaturated zone, negative water pressure is nonlinearly related to water saturation. Thus, Equation (1) represents a parabolic partial differential equation with p as the primary variable.

Equation (1) can be solved by a variety of numerical methods, including finite difference *e.g.* [1, 2], Galerkin finite element *e.g.* [3–5], mixed finite element *e.g.* [6, 7] and finite volume *e.g.* [8–11] approaches. While the finite difference method is often the preferred choice for one-dimensional problems, its application to multiple dimensions is limited to the domains of regular shape, which can be covered by rectangular grids. Many engineering applications, *e.g.* related to slope stability or seepage through earth dams and embankments, involve two-dimensional domains of complex shape, which can be efficiently discretized by triangulation. The obtained numerical grid can be used as a basis for either finite element or finite volume schemes. The latter group of methods is particularly appealing in view of their inherent conservative properties. Moreover, it has been shown that the finite element method with a consistent approximation of the mass storage term leads to oscillatory solutions [12]. In order to avoid this problem, diagonalization (lumping) of the mass matrix is commonly applied [4, 12], leading to discrete schemes similar to those resulting from the finite volume method.

In this paper, we present the application of the control volume finite element method to solving Equation (1). This method combines the features of the finite element and finite volume approaches *e.g.* [11, 13, 14]. We focus on two-dimensional problems with spatial domains discretized using unstructured triangular meshes.

2. Mesh generator

A two-dimensional unstructured mesh generator NetGen, developed by Burzyński, is based on the Delaunay triangulation algorithm *e.g.* [15]. It follows the implementations described in [16–18], but includes certain modifications, which allow to create anisotropic meshes. The triangulation is performed for a set of points in a plane, which define the outer boundary of the solution domain. It is possible to define disconnected domains or domains containing hollow spaces. Grid refinement is enforced by specifying the minimum length of the sides of the triangles adjacent to the boundary, as well as by introducing internal nodes, which remain fixed during the generation process.

The major modification with respect to the afore-mentioned mesh generators consists in introducing two weighting parameters in order to enable grid anisotropy. This is achieved by relaxing the criterion for checking the internal angles of triangular elements, *i.e.* certain obtuse triangles are permitted. Moreover, when a new point is inserted at a specified edge, its position is computed as a weighted average of the edge endpoints, and not as an arithmetic average, as commonly used. The values of the two weighting parameters w_1 and w_2 are specified by the user (*e.g.* $w_1 = 0.700$ and $w_2 = 0.577$ correspond to the standard algorithm producing almost equilateral triangles). The influence of these parameters on the resulting grid is shown in Example 3. However, large differences in node spacing or distorted element shapes may significantly influence the stability and accuracy of the numerical solution.

The mesh generator was dedicated to the problems of surface and subsurface water flow. Therefore, it is capable of local mesh refining, and of including spatially variable material properties (*e.g.* permeability in the case of flow in a porous medium). The NetGen generator was used in several applications *e.g.* [19, 20]. A graphic interface NetView allows to view and modify the mesh created by NetGen. Additionally, the Voronoi diagram can be generated for the obtained Delaunay triangulation.

3. Finite volume formulation

Unstructured grids generated by the above algorithm can be used as a basis for either cell-centred or vertex-centred finite volume schemes. In the first case, the discrete form of the conservation law is applied to control (finite) volumes corresponding to the elements of the primary grid [20, 21], with computational nodes located at their geometric centres. Since the line segment connecting the centres of two adjacent triangles is, in general, not orthogonal to their common edge (control volume face), estimation of the potential gradient using a finite-difference formula involving only the values from the two centres of neighbouring cells is usually inaccurate. The accuracy can be increased if the values from the endpoints of the edge (grid vertices) are taken into account. Since these values are not explicitly represented in the solution, they must be interpolated from the cell-centred values in all neighbouring cells using an appropriate reconstruction

procedure. This significantly adds to the overall complexity of the numerical algorithm.

In this work, we focus on an alternative approach, *i.e.* a vertex-centred scheme, where the conservation principle is enforced on a dual grid of polygonal control volumes built around the vertices of the primary triangular grid. A popular method of defining the control volumes is to join the midpoint of each edge of the primary grid with the barycentres of adjacent elements, *cf.* Figure 1. This method is often termed the median-dual method (MD). Another option is to use the Voronoi diagram (VD). In this case, the division points of the dual grid are the circumcentres of the respective elements (centres of circles circumscribed to the triangles). A useful property of the Voronoi diagram is that the segment which joins the circumcentres of two adjacent triangles is perpendicular to their common edge and crosses this edge at the midpoint. On the other hand, neither of the angles in the primary grid triangle should be obtuse, or else the circumcentre would be located outside the triangle.

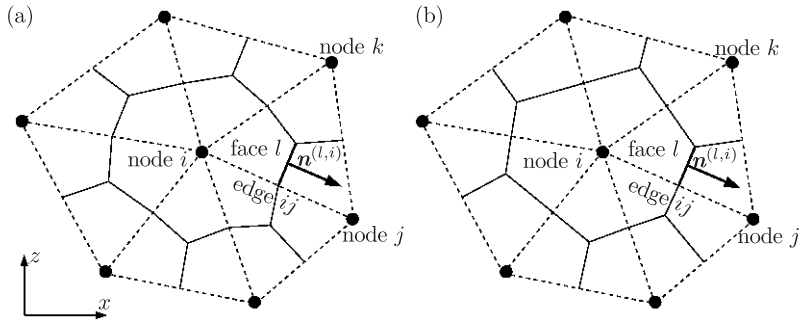

Figure 1. Finite volume dual grid constructed from a primary triangular grid according to the median-dual method (a) and the Voronoi diagram (b)

The starting point for the development of a finite volume scheme is the governing Equation (1) written in the integral conservative form for an arbitrary control volume V_i, enclosed by its boundary Γ_i:

$$\frac{\partial}{\partial t}\int_{V_i}(\phi S\rho)\,dV+\int_{\Gamma_i}(\rho\boldsymbol{v}\cdot\boldsymbol{n})\,ds=0 \tag{4}$$

where $\boldsymbol{n}$ is the unit vector normal to the control volume boundary and directed outwards. The storage term is approximated using the values of the unknown functions at the vertex inside the control volume:

$$\frac{\partial}{\partial t}\int_{V_i}(\phi S\rho)\,dV\approx|V_i|\,\frac{\partial}{\partial t}(\phi_i S_i\rho_i)=\frac{\partial M_i}{\partial t} \tag{5}$$

where ϕ_i, S_i and ρ_i depend in general on p_i, and M_i is the mass of water stored in the control volume. The boundary integral is equal to the sum of integrals taken over each control volume face F_l belonging to the boundary Γ_i:

$$\int_{\Gamma_i}(\rho\boldsymbol{v}\cdot\boldsymbol{n})\,ds=\sum_{F_l\in\Gamma_i}\int_{F_l}\left(\rho\boldsymbol{v}\cdot\boldsymbol{n}^{(l,i)}\right)ds \tag{6}$$

The integral of the mass flux over a specific face can be, in turn, approximated as:

$$\int_{F_l} \left(\rho \boldsymbol{v} \cdot \boldsymbol{n}^{(l,i)}\right) ds \approx -|F_l|\, \rho^{(l)}\, \frac{k_s^{(l)}\, k_r^{(l)}}{\mu} \left(\nabla p^{(l)} - \rho^{(l)} \boldsymbol{g}\right) \cdot \boldsymbol{n}^{(l,i)} = Q^{(l,i)} \tag{7}$$

where the superscript l denotes the variables evaluated at the considered face. Their computation will be presented on the example of face l located in the primary grid element ijk and adjacent to the primary grid edge ij (Figure 1).

The water pressure within the triangular element ijk is approximated using the finite element approach with linear shape functions. This results in a uniform value of the pressure gradient given by the following formulae:

$$\nabla_x p^{(l)} = B_x^{(i)} p^{(i)} + B_x^{(j)} p^{(j)} + B_x^{(k)} p^{(k)} \tag{8}$$

$$\nabla_z p^{(l)} = B_z^{(i)} p^{(i)} + B_z^{(j)} p^{(j)} + B_z^{(k)} p^{(k)} \tag{9}$$

where $B_\xi^{(m)}$ are geometry dependent coefficients, defined as follows:

$$B_x^{(i)} = \frac{z^{(j)} - z^{(k)}}{2\,A^{(ijk)}} \quad B_z^{(i)} = \frac{x^{(k)} - x^{(j)}}{2\,A^{(ijk)}} \tag{10}$$

$$B_x^{(j)} = \frac{z^{(k)} - z^{(i)}}{2\,A^{(ijk)}} \quad B_z^{(j)} = \frac{x^{(i)} - x^{(k)}}{2\,A^{(ijk)}} \tag{11}$$

$$B_x^{(k)} = \frac{z^{(i)} - z^{(j)}}{2\,A^{(ijk)}} \quad B_z^{(k)} = \frac{x^{(j)} - x^{(i)}}{2\,A^{(ijk)}} \tag{12}$$

where $A^{(ijk)}$ is the area of the element. Since we assume scalar permeability of the porous medium, the water flux normal to the face can be expressed as a product of a scalar transfer coefficient and the normal component of the gradient (for anisotropic medium, the tangential component of the gradient would be also required):

$$\nabla p^{(l)} \cdot \boldsymbol{n}^{(l,i)} = C^{(i)} p^{(i)} + C^{(j)} p^{(j)} + C^{(k)} p^{(k)} \tag{13}$$

where

$$C^{(i)} = B_x^{(i)}\, n_x^{(l,i)} + B_z^{(i)}\, n_z^{(l,i)} \tag{14}$$

$$C^{(j)} = B_x^{(j)}\, n_x^{(l,i)} + B_z^{(j)}\, n_z^{(l,i)} \tag{15}$$

$$C^{(k)} = B_x^{(k)}\, n_x^{(l,i)} + B_z^{(k)}\, n_z^{(l,i)} \tag{16}$$

For the Voronoi dual grid, the expression for the normal gradient component reduces to a simple finite difference formula, because the face is perpendicular to the edge:

$$\nabla p^{(l)} \cdot \boldsymbol{n}^{(l,i)} = -\frac{p^{(i)}}{L^{(ij)}} + \frac{p^{(j)}}{L^{(ij)}} \tag{17}$$

where $L^{(ij)}$ is the length of the edge. Therefore, the flux at each face depends only on two unknowns corresponding to the endpoints of the adjacent edge. In the median-dual approach, all three vertices of the triangle are involved in the approximating formula. In the special case of an equilateral triangle, the two schemes become identical.

The intrinsic permeability $k^{(l)}$ is constant within each element, while the relative permeability $k_r^{(l)}$ is variable and its average value must be computed. An intuitive (and common) approach is to take the arithmetic average of the values from all three nodes of the element [5, 3]:

$$k_r^{(l)} = \frac{1}{3}\left(k_r^{(i)} + k_r^{(j)} + k_r^{(k)}\right) \tag{18}$$

Alternatively, we can take the arithmetic average of the values from the endpoints of the edge adjacent to the considered face:

$$k_r^{(l)} = \frac{1}{2}\left(k_r^{(i)} + k_r^{(j)}\right) \tag{19}$$

The second formula is a natural choice for a VD scheme, since it retains the dependence of the flux on two points only, however, it can also be used with an MD discretisation. Apart from the arithmetic mean, there exist other two-point permeability approximations, which can be used with both MD and VD discretisations. A popular choice is the upwind (upstream) mean defined as follows [8, 11]:

$$k_r^{(l)} = \begin{cases} k_r^{(i)} & \text{if } \left(\nabla p^{(l)} - \rho^{(l)}\,\boldsymbol{g}\right)\cdot \boldsymbol{n}^{(l,i)} \le 0 \\ k_r^{(j)} & \text{if } \left(\nabla p^{(l)} - \rho^{(l)}\,\boldsymbol{g}\right)\cdot \boldsymbol{n}^{(l,i)} > 0 \end{cases} \tag{20}$$

The use of an upstream average is necessary when advection (gravity) forces dominate over diffusion (capillary) forces at the scale of a single grid cell. This occurs, for instance, when modelling infiltration into dry soil on a coarse grid [8]. Upwinding is also necessary in two-phase flow simulations [22]. If arithmetic averaging is used instead of upwinding, unphysical oscillations arise in the resulting pressure distribution. On the other hand, the upwind average is less accurate than the arithmetic average on finer grids. This problem was studied extensively for the case of one-dimensional unsaturated flow, and more accurate schemes have been proposed, *e.g.* [23]. Their evaluation for unstructured grids is beyond the scope of this paper and is the subject of ongoing work. Here, we focus on four approaches: MD-ARIT (median-dual grid with permeability evaluated according to Equation (18)), MD-UPW (median-dual grid with permeability upwinding), VD-ARIT (Voronoi dual grid with permeability given by Equation (19)) and VD-UPW (Voronoi dual grid with permeability upwinding).

Spatial discretization results in a system of differential equations with respect to time. The integration in time is performed with a fully implicit Euler scheme, *i.e.* the flux terms are evaluated using the unknown pressure values from the next time level:

$$\frac{M_i^{t+\Delta t} - M_i^t}{\Delta t} + \sum_{F_l \in \partial V_i} Q_{l,i}^{t+\Delta t} = 0 \tag{21}$$

The obtained system of nonlinear algebraic equations is solved using the Newton iterative method with line search. The entries of the Jacobian matrix are obtained by numerical differentiation. The iterations are stopped when the changes in the value of water saturation at the unsaturated nodes are smaller than $1.0 \cdot 10^{-4}$ and

the changes in the value of water pressure at the saturated nodes are smaller than 1 Pa. The time step is adjusted during the solution in order to keep the required number of iterations for each time step in the range of 3 to 7.

The algorithm described here can be easily extended to the case of axisymmetric flow in the coordinate system r–z. In such a case, it is only necessary to replace the two-dimensional volume V_i with the volume of a three-dimensional figure obtained by rotation about the z axis. Similarly, the length of the face F_l should be replaced with the area of the corresponding surface of revolution.

4. Examples

4.1. Example 1: Comparison with analytical solution

In the first example, the results of numerical simulations are compared with the analytical solution developed by Tracy [24]. The solution domain is a square of the dimensions of $X = 1\,\mathrm{m}$ by $Z = 1\,\mathrm{m}$ (Figure 2). The fluid is assumed to be incompressible ($\rho = 10^3\,\mathrm{kg\,m^{-3}}$, $\mu = 10^{-3}\,\mathrm{Pa\,s}$) and the porous medium is rigid ($\phi = 0.45$, $k_s = 1.0194 \cdot 10^{-12}\,\mathrm{m^2}$). The hydraulic functions have exponential form:

$$S = S_r + (1 - S_r)\exp(-\alpha p) \tag{22}$$

$$k_r = \exp(-\alpha p) \tag{23}$$

with $S_r = \frac{1}{3}$ and $\alpha = 2.5484 \cdot 10^{-5}\,\mathrm{Pa^{-1}}$. Uniform distribution of water pressure $p_0 = -9.81 \cdot 10^5\,\mathrm{Pa}$ was assumed as the initial condition and this value was kept constant throughout the simulation along the bottom and the vertical sides of the domain. At the top boundary a sinusoidal distribution of pressure was imposed:

$$p(x, z = L_z, t) = \frac{1}{\alpha}\ln\left(\exp(\alpha p_0) + (1 - \exp(\alpha p_0))\sin\left(\frac{\pi x}{X}\right)\right) \tag{24}$$

Under the above assumptions, the value of water pressure for a given spatial point (x, z) and time t can be calculated analytically as [24]:

$$p(x,z,t) = \frac{1}{\alpha}\ln\left\{\exp(\alpha p_0) + \bar{p}\sin\left(\frac{\pi x}{L_x}\right)\exp\left(\alpha(Z - z)/2\right)\right. \\ \left.\left[\frac{\sinh(\beta z)}{\sinh(\beta Z)} + \frac{2}{Z c}\sum_{n=1}^{\infty}(-1)^n\frac{\lambda_n}{\gamma}\sin(\lambda_n z)\exp(-\gamma t)\right]\right\} \tag{25}$$

where $c = \frac{\alpha\phi(1-S_r)}{k_s}$, $\gamma = (\beta^2 + \lambda_n^2)/c$, $\beta = \sqrt{\frac{\alpha^2}{4} + \left(\frac{\pi}{X}\right)^2}$, $\bar{p} = 1 - \exp(\alpha p_0)$ and $\lambda_n = \frac{n\pi}{Z}$.

Three spatial grids were considered, with the node spacing along the boundary equal to 25 cm, 10 cm and 2 cm, respectively. The simulation time was 180 s, while the time step was allowed to vary between 10^{-3} s and 1 s according to the performance of the iterative solver.

The spatial distribution of water pressure at the end of the simulation is shown in Figure 3 for the MD-ARIT and MD-UPW schemes and the medium grid size. It can be seen that the MD-ARIT method produced results closer to the analytical solution, while the MD-UPW scheme led to a slightly faster propagation

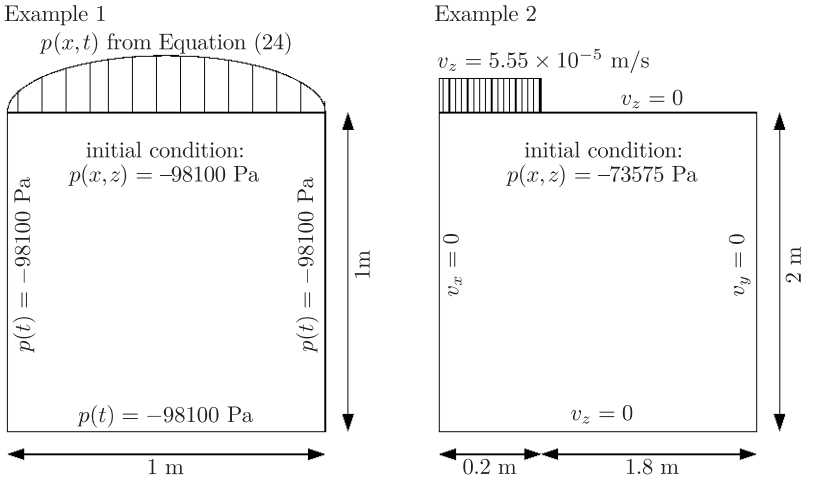

Figure 2. Geometry and boundary conditions for Example 1 and 2

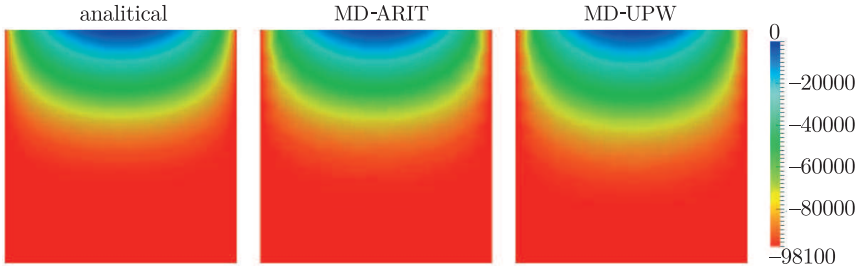

Figure 3. Example 1, distribution of water pressure according to the analytical solution and the MD-ARIT and MD-UPW solutions on the medium grid

of the infiltration front. In this case, the upwinding of relative permeabilities leads to larger values of permeability at the control volume face than arithmetic averaging. This is confirmed by Figure 4, which shows the profile of water pressure along the vertical symmetry axis of the solution domain for the final time $t = 180$ s. Schemes based on arithmetic averaging are more accurate than schemes based on upwinding. On the other hand, if the same method is used for permeability averaging, the differences between the schemes based on the median-dual grid and Voronoi dual grid are very small.

The accuracy of various schemes can be evaluated in terms of the root mean square error (RMSE) of the pressure head:

$$R = \sqrt{\frac{1}{N}\sum_{1}^{N}(p_{num} - p_{ref})^2} \tag{26}$$

where N is the number of internal nodes in the domain, p_{num} is the final water pressure at a specific node from the numerical solution, and p_{ref} is the corresponding pressure value from the analytical solution. The values of the RMSE

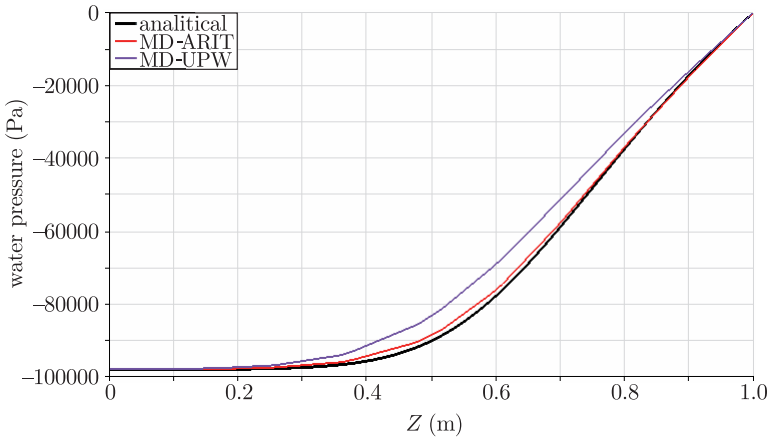

Figure 4. Example 1, water pressure profile along the vertical symmetry axis, according to the analytical solution and the MD-ARIT and MD-UPW solutions on the medium grid

Table 1. Root mean square error for various discretization schemes used in Example 1

Δx(m)	MD-ARIT	VD-ARIT	MD-UP	VD-UP
0.25	2061	2600	7413	7342
0.1	742.6	813.2	4082	4040
0.02	47.68	49.20	903.5	900.1

are listed in Table 1. The upwind schemes are less accurate than arithmetic averaging for the entire range of discretization. Nevertheless, all schemes are convergent, *i.e.* the error decreases with a decrease in the size of grid cells.

4.2. Example 2: Infiltration in uniformly grained sand

The second example concerns downward infiltration in sand with a prescribed infiltration flux on a part of the soil surface (Figure 2). The soil is characterized by the Brooks-Corey-Burdine hydraulic functions of the following form:

$$S = S_r + (1 - S_r)S_e \tag{27}$$

$$S_e = \begin{cases} (p/p_e)^{-\lambda} & \text{if } p < p_e \\ 1 & \text{if } p \geq p_e \end{cases} \tag{28}$$

$$k_r = S^{3+2/\lambda} \tag{29}$$

where S_e is the effective (normalized) water saturation, $S_r = 0.096$ is the residual water saturation, $p_e = -696\,\text{Pa}$ is the air entry pressure, and $\lambda = 2.5$ is a parameter related to the uniformity of grain size. The assumed value of λ corresponds to a medium with a relatively uniform pore-size distribution and leads to a rapid decrease in the values of water saturation in the pressure range slightly above p_e, which in turn produces a very steep infiltration front. The infiltrating mass flux is slightly smaller than the soil infiltration capacity so that ponding of water on the surface is avoided. The compressibility of water and of the porous medium is neglected.

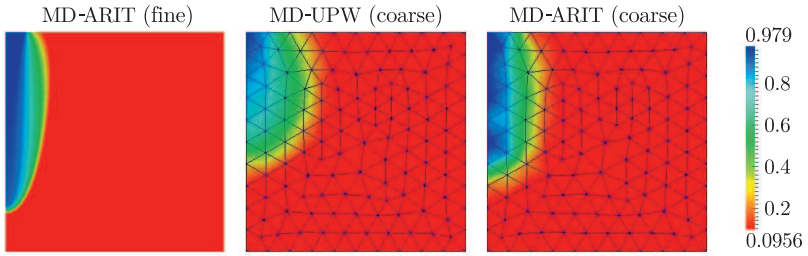

Figure 5. Example 2, distribution of water saturation for different grids and permeability averaging schemes

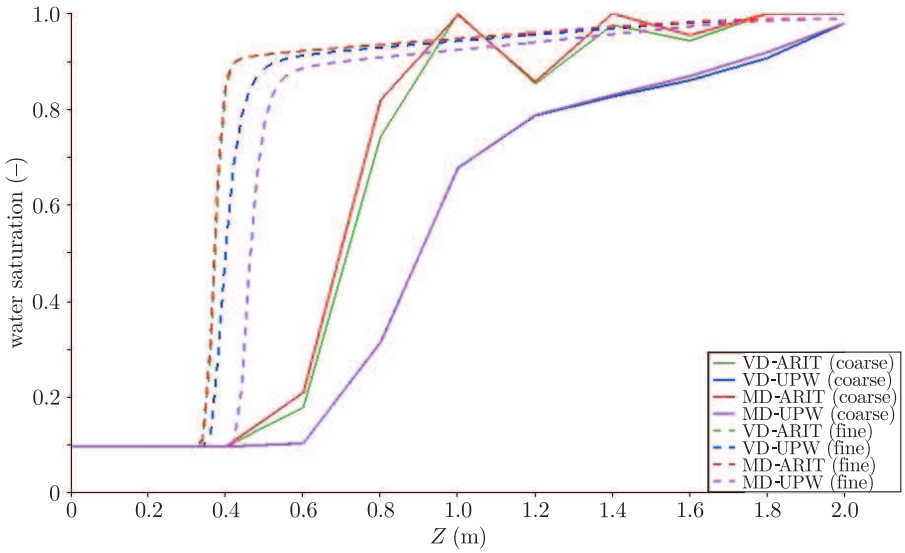

Figure 6. Example 2, water saturation profiles along $x = 0$ for different grids and permeability averaging schemes

Numerical results are presented for two grids – a fine grid with a node spacing of 0.02 m along the boundaries, and a coarse grid with a node spacing of 0.2 m. Figure 5 shows the distribution of water saturation in the domain after 4 hours of infiltration. The fine-grid solution shows a very steep infiltration front with a rapid transition between the dry and wet zones. In contrast, the coarse grid solutions are characterized by more diffuse wetting fronts. This is particularly visible for the MD-UPW solution. In the MD-ARIT solution, the wetting front is less diffused and the shape of the wet zone corresponds better to the fine grid solution. However, the use of arithmetic averaging leads to non-physical oscillations in the pressure and saturation profiles. This can be seen in Figure 6, which presents the saturation profiles along $x = 0$. On the coarse grid, the ARIT and UPW schemes lead to qualitatively very different results. The UPW schemes produce smoothed and oscillation-free fronts, overestimate the infiltration velocity in the horizontal direction and significantly underestimate the velocity in the vertical direction. On the other hand, the ARIT schemes are more accurate with

regard to the position of the wetting front, but show significant oscillations. In a way, these two schemes can be thought of as equivalents of the upwind and central difference schemes for the advection equation. It is well known *e.g.* [25] that the centred scheme is characterized by numerical dispersion, which leads to oscillations, while the upwind scheme introduces strong numerical diffusion, which leads to a smoothing of the wetting front and damps any oscillations. Figure 6 shows that these numerical errors decrease as the grid is refined. Similarly to the previous example, if the same permeability averaging method is used, both the MD and VD schemes produce similar results.

4.3. Example 3: Seepage through a dike

Here, we consider flow in a dike and in the surrounding soil caused by a rapid increase in water level in a river due to a flood wave. The geometry of the domain is shown in Figure 7. Hydrostatic distribution of water pressure is assumed as the initial condition, with the groundwater table ($p=0$) located 5 m above the bottom of the domain. The water level on the left-hand side of the embankment is rapidly raised up to 1 m below the top of the embankment, and is maintained constant during the simulation. On the right-hand slope of the dike and at the soil surface behind it, a seepage face boundary condition is imposed. This means that the water can flow out freely when the water pressure in the porous medium reaches 0. Technically, this is achieved by specifying a Neumann boundary condition $\boldsymbol{v}\cdot\boldsymbol{n}=0$, as long as the soil remains unsaturated ($p<0$). When the pressure reaches 0, the condition is changed to the Dirichlet boundary condition, and $p=0$ is maintained, thus preventing a build-up of positive pressure values in the porous medium.

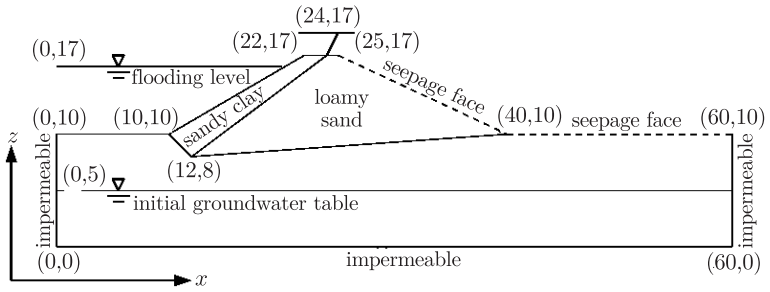

Figure 7. Geometry and boundary conditions for Example 3

The solution domain consists of three different soils, characterized by the van Genuchten-Mualem hydraulic functions of the following form:

$$S = S_r + (1-S_r)S_e \tag{30}$$

$$S_e = \begin{cases} \left(1+(p/p_g)^{1/(1-m)}\right)^{-m} & \text{if } p<0 \\ 1 & \text{if } p\geq 0 \end{cases} \tag{31}$$

$$k_r = S_e^{1/2}\left(1-(1-S_e^{1/m})^m\right)^2 \tag{32}$$

The values of the parameters are listed in Table 2. The domain was discretized using NetGen, with three sets of parameters w_1 and w_2. In each case, the spacing of the nodes at the boundaries was identical, however, the total number of nodes in the domain differed significantly (see Table 3 and Figures 8–9). Grid 1 consists of elements similar to equilateral triangles, while the triangles composing Grid 3 are considerably stretched in the vertical direction. The simulations were performed using only the MD-ARIT approach.

Table 2. Soil parameters used in Example 3

soil	ϕ (–)	S_r (–)	p_g (Pa)	m (–)	k_s (m^2)
sand	0.43	0.105	−680	0.627	$8.25 \cdot 10^{-12}$
loamy sand	0.41	0.139	−794	0.561	$4.05 \cdot 10^{-12}$
sandy clay	0.38	0.263	−3636	0.187	$3.33 \cdot 10^{-14}$

Table 3. Grid parameters used in Example 3

grid	w_1	w_2	nodes	elements	edges
1 (fine)	0.700	0.577	1518	2859	4376
2 (medium)	1.500	0.577	733	1289	2021
3 (coarse)	2.000	2.000	365	545	905

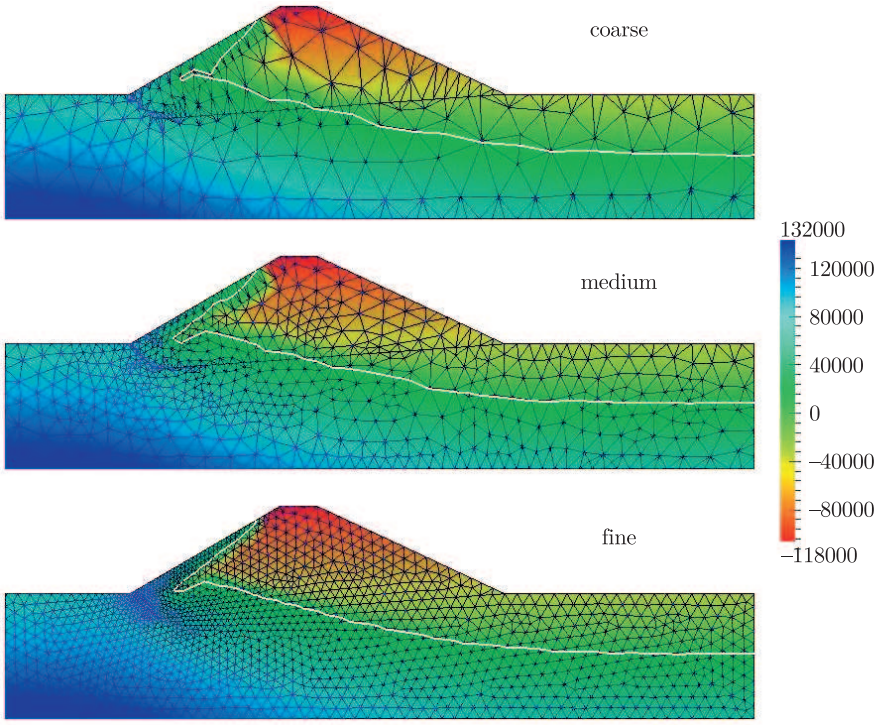

Figure 8. Example 3, water pressure distribution at $t = 27.8$ h. The solid white line represents the groundwater table ($p = 0$ isoline)

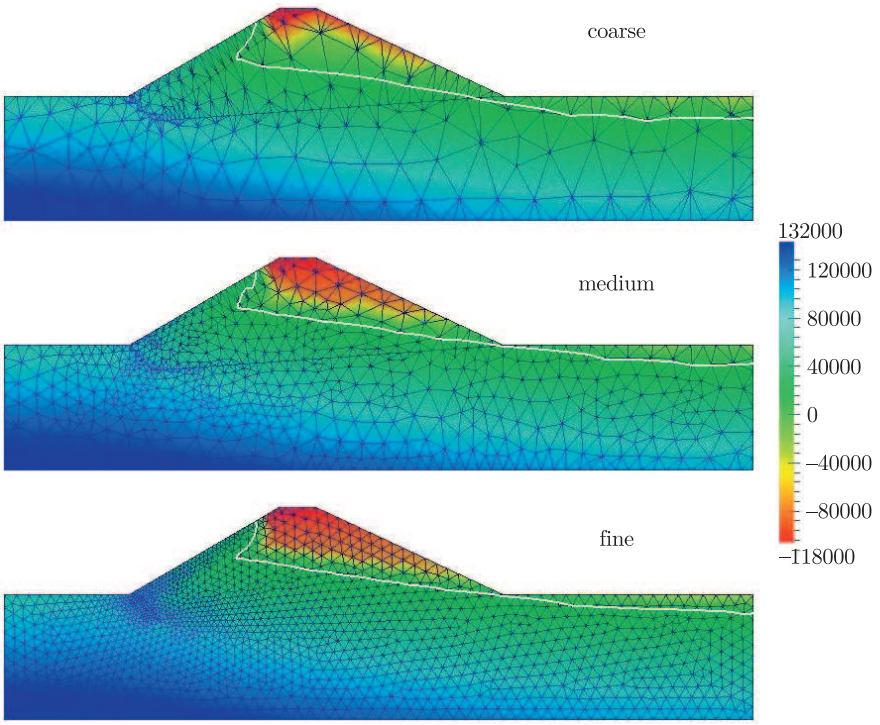

Figure 9. Example 3, water pressure distribution at $t = 111.1\,\mathrm{h}$. The solid white line represents the groundwater table ($p = 0$ isoline)

Figures 8 and 9 show the distribution of the water pressure at time $t = 27.8\,\mathrm{h}$ and $t = 111.1\,\mathrm{h}$, respectively. The position of the groundwater table is denoted with a solid white line. Due to the presence of a weakly permeable clay screen on the outward slope of the dike, water enters the main body of the dike mainly from the underlying sand layer, Figure 8. With time, the groundwater level in the sand layer and in the dike rises and approaches the soil surface in the vicinity of the base of the right-hand slope of the dike. According to the medium and fine grid simulations, at $t = 111.1\,\mathrm{h}$ water begins to flow out at this location, while the coarse grid simulation predicts a somewhat delayed outflow, at about $t = 120\,\mathrm{h}$. This difference is caused by the fact that the coarse grid solution leads to a higher saturation in the main body of the dike due to overestimated upward infiltration. The differences in the results between the medium and fine grid are less pronounced. As can be expected from the number of nodes, the computational times differ significantly. For the fine grid, the calculations took 4717 s, whereas for the medium grid – 808 s, and for the coarse grid 288 s.

5. Conclusions

We presented a numerical algorithm for solving the equation describing two-dimensional flow in a variably saturated porous medium. The algorithm is based

on a primary triangular mesh, from which a dual control volume mesh is created. The algorithm enables several choices with respect to the approximation of the average relative permeability at the control volume faces. Numerical experiments showed that the method used for permeability averaging significantly affects the results. On the other hand, the differences between the dual grids obtained by the median-dual method and by the Voronoi method were rather small, when the same permeability averaging scheme was employed.

References

[1] Clement T P, Wise W R and Molz F J 1994 *J. Hydrology* **161** (1–4) 71
[2] Simpson M J and Clement T P 2003 *J. Hydrology* **270** (1–2) 49
[3] Zaradny H 1993 *Groundwater Flow in Saturated and Unsaturated Soil*, Balkema, Rotterdam
[4] Celia M A, Bouloutas E T and Zarba R L 1990 *Water Resour. Res.* **26** (7) 1483 (doi: 10.1029/WR026i007p01483)
[5] Tracy F T 2010 *The Open Hydrology Journal* **4** 227
[6] Bause M and Knabner P 2004 *Adv. Water Resour.* **27** 565
[7] Fahs M, Younes A and Lehmann F 2009 *Environ. Modell. Softw.* **24** (9) 1122
[8] Forsyth P A, Wu Y S and Pruess K 1995 *Adv. Water Resour.* **18** (1) 25 (doi: 10.1016/0309-1708(95)00020-J)
[9] Fuhrmann J and Langmach H 2001 *Appl. Num. Math.* **37** (1–2) 201
[10] Rees I, Masters I, Malan A G and Lewis R W 2004 *Comput. Meth. Appl. Mech. Eng.* **193** (42–44) 4741
[11] Cumming B, Moroney T and Turner I 2011 *A Mass-conservative Control Volume-finite Element Method for Solving Richards Equation in Heterogeneous Porous Media*, BIT Numerical Mathematics (doi: 10.1007/s10543-011-0335-3)
[12] Ju S-H and Kung K-J S 1997 *Comput. Geosci.* **23** (2) 175
[13] Helmig R 1997 *Multiphase Flow and Transport Processes in the Subsurface: a Contribution to the Modeling of the Hydrosystems*, Springer-Verlag
[14] Voller V R 2009 *Basic Control Volume Finite Element Methods for Fluids and Solids*, World Scientific
[15] Frey P J and George P-L 2008 *Mesh Generation. Application to Finite Elements*, Wiley
[16] Shewchuk J R 2005 *Triangle. A Two-dimensional Quality Mesh Generator and Delaunay Triangulator. Ver. 1.6*, Carnegie Mellon University, US (http://www.cs.cmu.edu/~quake/triangle.html)
[17] Niceno B 1996 *Easy Mesh. A Two-dimensional Quality Mesh Generator. Ver. 1.4*, University of Trieste, Italy (http://www-dinma.univ.trieste.it/nirftc/research/easymesh/)
[18] Müller J D 1996 *On Triangles and Flow*, PhD Thesis, University of Michigan
[19] Szydłowski M (Ed.) 2003 *Mathematical Modeling of Hydraulic Effects of Dam Breaks*, KGW PAN (in Polish)
[20] Szymkiewicz A and Burzyński K 2007 *TASK Quart.* **11** (4) 397
[21] Manzini G and Ferraris S 2004 *Adv. Water Resour.* **27** 1199 (doi: 10.1016/j.advwatres.2004.08.008)
[22] Helmig R and Huber R 1998 *Adv. Water Resour.* **21** (8) 697 (doi: 10.1016/S0309-1708(97)00023-7)
[23] Szymkiewicz A 2009 *Water Resour. Res.* **45**, W10403 (doi: 10.1029/2008WR007654)
[24] Tracy F T 2006 *Water Resour. Res.* **42**, W08503 (doi: 10.1029/2005WR004638)
[25] Szymkiewicz R 2010 *Numerical Modeling in Open Channel Hydraulics*, Springer